Effect of electrical boundary conditions on the polarization distribution around a crack in a ferroelectric single domain

Jie Wang[a,b*] and Marc Kamlah[b]
[a]Institute of Applied Mechanics, School of Aeronautics & Astronautics, Zhejiang University
Hangzhou, Zhejiang 310027, China
[b]Karlsruhe Institute of Technology (KIT), Institute for Materials Research II
Postfach 3640, 76021 Karlsruhe, Germany

Abstract

In the present work, polarization distributions around an open crack with different electrical boundary conditions in a single crystal ferroelectric are investigated by using a phase field model. The surface effect of polarization is taken into account in the phase field model, which has not been included in previous ferroelectric crack models. The simulation results show that the impermeable crack and the crack filled with air have a significant influence on the polarization distribution, while the permeable and the crack filled with water have little influence. It is also found that the zero boundary condition of polarization increases the influence of the crack on the permeable crack and the crack filled with water. The results of the present work suggest that a crack filled with air can be approximated as an impermeable crack, and a crack filled with water can be regarded as a permeable crack in ferroelectric materials.

* Corresponding author. Tel: +86 571 87953110, Fax: +86 571 87952651.
E-mail address: jw@zju.edu.cn

1. Introduction

Ferroelectric materials have received considerable attention in the industry and the academia due to their distinguished piezoelectric, dielectric and ferroelectric properties. The piezoelectric or inverse piezoelectric effect of ferroelectric materials is highly dependent on the polarization distribution. The piezoelectric constant in ferroelectric materials is inhomogeneous before poling and determined by locally electrical polarization. Without any external loadings, the electrical polarization is called spontaneous polarization, which is a function of temperature for a given material system. When large external loadings and/or different boundary conditions are applied on ferroelectrics, the distribution of spontaneous polarization may change. Correspondingly, the piezoelectric properties will be changed. Thus, the piezoelectric properties of ferroelectric materials are not only dependent on the nature of the material but also on the external loadings and boundary conditions. In general, it requires three physical fields, namely polarization field, electric field and strain field, to describe the nonlinear electromechanical behavior of ferroelectric materials under external loadings and different boundary conditions [1].

Ferroelectric materials often possess defects, such as notches and cracks. The presence of these defects will also greatly influence the polarization distribution inside the materials. For example, the different electrical boundary conditions on the surfaces of notches or cracks can change the polarization distribution through the strong depolarization field, which is induced by the spatial discontinuity of polarization. Because of the change of polarization, the piezoelectric constant around the cracks is changed completely. As a result, the electromechanical coupling behavior in front of the crack tip is changed. Based on different crack surface boundary conditions, the predictions from linear piezoelectric fracture mechanics are totally different [2-7]. Due to the change of polarization around the crack tip,

the theoretical results based on linear piezoelectric fracture mechanics cannot predict the experimental observations of the fracture behavior of ferroelectric ceramics under mechanical and/or electrical loading [8-9]. Therefore, the nonlinear analysis on the polarization distribution around the notches or cracks with different electrical boundary conditions is needed for studying the fracture behavior of ferroelectric materials. To investigate the nonlinear behavior of ferroelectrics, different phenomenological models have been proposed [10-13]. In the phenomenological models, the total polarization in ferroelectric materials is often divided into reversible and irreversible parts. The reversible part is a function of the external mechanical and electrical loadings, while the irreversible part depends on the loading history via internal state variables. Recently, phase field models have also been employed to study the nonlinear behavior of ferroelectrics [14-16]. In the phase field models, the polarization is regarded as an order parameter which can change its orientation and magnitude under the external mechanical and electrical loadings. In the present work, we employ a 3D finite-element based phase field model to study the polarization distribution around an open crack with different electrical boundary conditions in a single crystal ferroelectric plate with single domain. The 3D finite-element based phase field model was previously employed to study the polarization distribution in ferroelectric nanostructures [17-18]. In the present work, the surface effect of polarization and different crack electrical boundary conditions are taken into account, which has not been studied in the previous simulations.

2. Electrical boundary conditions for an open crack

The electrical boundary conditions on crack surface have a significant influence on the polarization distribution and the fracture behavior of ferroelectric materials. For an open crack, the electrical boundary condition of crack surface depends on the medium inside the crack. For example, if the medium inside the crack is conductive, the electric potential φ on the crack surface will be constant,

$$\varphi = 0, \quad \text{(conductive crack)} \tag{1}$$

which is so-called conductive crack. If the medium is a dielectric, there exist three kinds of electrical boundary conditions on the crack surface: permeable crack; semi-permeable crack; and impermeable crack, which depend on the dielectric constant of the medium. If the dielectric medium is a fluid, there is no elastic energy inside the crack but there exists an electrically internal energy due to the presence of electric field, which can be expressed as

$$U_E = \frac{1}{2} D_i E_i = \frac{1}{2} \kappa_c E_i E_i , \tag{2}$$

where κ_c is the dielectric constant of the medium, and D_i and E_i are the electric displacement and electric field, respectively. For an infinite large κ_c , the electric displacement can penetrate the crack and the normal components of electric displacement D_n are the same on upper and lower crack surface. This will result in a permeable crack,

$$D_n^+ = D_n^- \quad \text{and} \quad \varphi^+ = \varphi^- , \tag{3}$$

in which superscripts + and - denote the upper and lower surfaces, respectively. If κ_c approaches zero, the crack becomes impermeable. In this case, the electrical boundary condition is

$$D_n^+ = D_n^- = 0 \quad \text{and} \quad \varphi^+ - \varphi^- \neq 0 . \tag{4}$$

If the dielectric constant κ_c has a finite value, the crack is called semi-permeable and the corresponding electrical boundary condition becomes

$$D_n^+ - D_n^- = -\kappa_c \frac{\varphi^+ - \varphi^-}{u^+ - u^-} \tag{5}$$

In the present work, the influence of three kinds of electrical boundary condition on the polarization distribution around the crack is investigated. For an impermeable crack, the dielectric constant κ_c is assumed to be zero. The dielectric constant κ_c is taken as $10^6 \kappa_0$ to approximate a permeable crack in which κ_0 is the dielectric constant of air. The crack is

assumed to be filled with different dielectric fluids to model the semi-permeable crack. Furthermore, three kinds of dielectric fluids are studied for the semi-permeable crack, which are water with $\kappa_c = 80\kappa_0$, silicon oil with $\kappa_c = 2.5\kappa_0$ and air with $\kappa_c = \kappa_0$.

3. Surface effect on polarization

Due to the symmetry breaking on the surface of ferroelectric crystal, polarizations on surfaces are different from those inside the crystal. This is the surface effect of polarization, which is different from the electrical boundary conditions mentioned in Section 2. The different electrical boundary conditions are related to the electric displacement on crack surface while the surface effect of polarization is only related to the polarization. The relation of electric displacement and polarization can be expressed as $D_i = \kappa_0 E_i + P_i$. With the size decreasing, the surface effect becomes significant. In the study of small size ferroelectrics, the surface effect can be included in continuum theories by setting appropriate boundary conditions of polarization. The boundary condition for polarization, P_{i}, is usually given by

$$\frac{dP_i}{dn} = -\frac{P_i}{\delta_i}, \ (i = 1,2,3) \tag{6}$$

where n refers to a unit length in the outward normal direction of the surface and δ_i is the so-called extrapolation length, which is introduced to describe the difference of polarizations between the surface and the interior of the material. Figure 1 schematically shows the surface effect on ferroelectric surface, in which P_i and P_∞ are the polarization at the surface and the inside, respectively. The polarization is reduced at the surface when δ_i is positive or zero, while the polarization is enhanced at the surface when δ_i is negative. Therefore, the value of δ_i determines the intrinsic size effect. When δ_i approaches infinity, the boundary condition becomes

$$\frac{dP_i}{dn} = 0, \ (i = 1,2,3) \tag{7}$$

which is called the free-polarization boundary condition [19], and the intrinsic size effect vanishes because in this case, there is no difference for polarizations in the media between the surface and the interior. When δ_i equals zero, polarizations are completely suppressed at the surface, i.e.,

$$P_i = 0\,,\ (i = 1,2,3) \tag{8}$$

which is called the zero-polarization boundary condition [19], thereby generating the most significant size effect. For an open crack in ferroelectrics, the effect of crack surface on polarization is similar to that of the material surface. In the present study, the free-polarization and zero-polarization boundary conditions are employed on the crack surface, respectively, to investigate how the surface effect changes the polarization distribution around the crack with different electrical boundary conditions.

4. Simulation methodology

In the present study, different electrical enthalpies are applied to the crack fluid medium and the ferroelectrics, respectively. For the crack medium, the electrical enthalpy is obtained from the electrically internal energy of Eq.(1), which is a function of electric field E_i and can be expressed as

$$h_c(E_i) = U_E - D_i E_i = -\frac{1}{2}\kappa_c E_i E_i\,, \tag{9}$$

The electrical enthalpy of crack h_c has to satisfy the following electrostatic equilibrium equation

$$\frac{\partial}{x_i}\left(-\frac{\partial h_c}{\partial E_i}\right) = 0\,. \tag{10}$$

For the ferroelectric medium, there exists Landau energy and elastic energy due to the presence of polarization field and strain field in the material. Therefore, the electrical enthalpy of ferroelectrics is a function of polarization P_i, strain ε_{ij} and electric field E_i, which can be expressed as

$$\begin{aligned} h(P_i, \varepsilon_{ij}, E_i) = \alpha_i P_i^2 + \alpha_{ij} P_i^2 P_j^2 + \alpha_{ijk} P_i^2 P_j^2 P_k^2 + \tfrac{1}{2} c_{ijkl} \varepsilon_{ij} \varepsilon_{kl} - q_{ijkl} \varepsilon_{ij} P_k P_l \\ + \tfrac{1}{2} g_{ijkl} (\partial P_i / \partial x_j)(\partial P_k / \partial x_l) - \tfrac{1}{2} \kappa_0 E_i E_i - E_i P_i, \end{aligned} \tag{11}$$

The first three terms in Eq. (11) represent the Landau energy, where $\alpha_1 = (T - T_0)/2\kappa_0 C_0$ is the dielectric stiffness, α_{11}, α_{12}, α_{111}, α_{112}, and α_{123} are higher order dielectric stiffnesses, T and T_0 denote the temperature and the Curie-Weiss temperature, respectively, C_0 is the Curie constant. The Landau energy is due to the phase transition from paraelectric phase to ferroelectric phase when the temperature decrease to below Curie temperature, which is independent of external electric field. The fourth term denotes the elastic energy of the system, in which c_{ijkl} are the elastic constants. The fifth term denotes the coupling energy between the polarizations and the strains, where q_{ijkl} are the electrostrictive coefficients. The sixth term is the gradient energy, in which g_{ijkl} are the gradient coefficients, and $\partial P_i / \partial x_j$ denotes the derivative of the *i*th component of the polarization vector, P_i, with respect to the *j*th coordinate, x_j, and *i*, *j* =1, 2, 3. The gradient energy gives the energy penalty for spatially inhomogeneous polarization. All the energy terms in Eq. (11) are the same as those in Ref. [20]. The last two terms are introduced through Legendre transformation to obtain the electrical enthalpy. With the electrical enthalpy, the stresses and electric displacements can be derived as $\sigma_{ij} = \partial h / \partial \varepsilon_{ij}$ and $D_i = -\partial h / \partial E_i$. The form of Eq.(11) can be reduced to the form of Eq.(9) for air with $\kappa_c = \kappa_0$ if the polarization and strain are zero.

In the phase field model of ferroelectrics, the temporal evolution of the polarization formation in ferroelectrics can be obtained from the following time-dependent Ginzburg-Landau equation

$$\frac{\partial P_i(\mathbf{x},t)}{\partial t} = -L\frac{\delta F}{\delta P_i(\mathbf{x},t)} \quad (i=1, 2, 3), \tag{12}$$

where L is the kinetic coefficient, $F = \int_V h + D_i E_i dv$ is the total free energy of the simulated system, $\delta F / \delta P_i(\mathbf{x},t)$ represents the thermodynamic driving force for the spatial and temporal evolution of the simulated system, $\mathbf{x}$ denotes the spatial vector, $\mathbf{x} = (x_1, x_2, x_3)$, and t is time. In addition to Eq. (12), the following mechanical equilibrium equation

$$\frac{\partial}{x_j}\left(\frac{\partial h}{\partial \varepsilon_{ij}}\right) = 0 \tag{13}$$

and Maxwell's (or Gauss') equation

$$\frac{\partial}{x_i}\left(-\frac{\partial h}{\partial E_i}\right) = 0 \tag{14}$$

must be satisfied at the same time for charge and body force free ferroelectric materials, in which the repeated indices imply summing over 1, 2 and 3. A nonlinear multi-field coupling finite element formulation is developed to solve the governing equations (12), (13) and (14). The finite element formulation is based on the weak form

$$\begin{aligned} &\int_V \frac{\partial h}{\partial \varepsilon_{ij}}\delta\varepsilon_{ij} + \frac{\partial h}{\partial E_i}\delta E_i + \frac{1}{L}\frac{\partial P_i}{\partial t}\delta P_i + \left[\frac{\partial h}{\partial P_i} + \frac{\partial}{\partial x_j}\frac{\partial h}{\partial P_{i,j}}\delta P_i\right] dv \\ &= \int_S \tau_i \delta u_i - \omega\delta\phi + \frac{\partial h}{\partial P_{i,j}} n_j \delta P_i dA \end{aligned}, \tag{15}$$

of the governing equations where τ_i is the surface traction, ω is the surface charge. $\frac{\partial h}{\partial P_{i,j}} n_j$ is the surface gradient flux, where n_j denotes the components of the normal unit vector of the surfaces. For the space discretization, an eight-node brick element with seven degrees of

freedom at each node is employed. The seven degrees of freedom are three displacements, electrical potential and three polarization components. The detailed derivation of the three-dimensional finite element formulation can be found in our previous work [1].

5. Simulation results and discussion

A 3D $PbTiO_3$ ferroelectric single crystal plate with the in-plane size of 120nm × 90nm and the thickness of one nm is studied in the present simulation, which is similar to a plane stress problem. Although the thickness is far smaller than the size of in-plane, three-dimensional brick elements are employed. In thickness direction, one element thickness equals to the plate thickness, i.e. only one element is employed in thickness x_1 direction. Fig.2. shows the mesh partition of the simulated ferroelectric plate in x_1=0 plane. The x_1 axis is normal to the paper plane and pointing outside. The mesh partition in x_1=1 nm plane is exactly same as Fig.2 because only one element is used in x_1 direction. Fig.2. (a) denotes the global mesh and Fig.2 (b) is the refined mesh around the crack tip and the green area denotes the crack medium. The crack is also partitioned and is assumed to be filled with fluids. The initial polarization of P_o=0.757 C/m^2 is along x_3 positive direction. The materials parameters of ferroelectrics is the same as those in Ref.[17]. The temperature in the simulations is room temperature. The upper and lower boundaries of the ferroelectric plate are short-circuited and other boundaries are open-circuited so that the initial polarization is uniform and stable if there is no crack. All boundaries of the ferroelectric plate are assumed to be stress-free. The crack is located in the middle of the ferroelectric plate. For different crack electrical boundary conditions, we use different dielectric constants as discussed in Section 2. For surface effect of polarization discussed in Section 3, the zero-polarization boundary condition corresponds to the boundary condition $P_i = 0$ at crack surfaces in Eq.(15), and free-polarization boundary

condition corresponds to zero gradient flux, i.e. $\frac{\partial h}{\partial P_{i,j}} n_j = 0$, at surface in the right hand side of Eq.(15). Therefore, we can use $P_i = 0$ and $\frac{\partial h}{\partial P_{i,j}} n_j = 0$ to model the zero-polarization and free-polarization boundary conditions, respectively.

Fig.3.(a) and Fig.3.(b) show the polarization distributions around electrically permeable cracks for free-polarization and zero-polarization boundary conditions, respectively. Due to the thickness of the simulated ferroelectric plate is far smaller than in-plane size, the results remain unchanged in thickness direction. So we only report the results at x_1=0. All units are nanometer in the figure. Only part of the polarizations around the crack is plotted in the figures for clarity. The polarizations far from the crack almost remain unchanged. For the free-polarization boundary condition, the crack has little influence on the polarization distribution. When the zero-polarization boundary condition is applied on the crack surfaces, it can be found that the polarization distribution has some changes in orientation. The influence of zero-polarization boundary condition on the polarizations around the crack can be clearly seen from Fig.4. Fig.4.(a) and Fig.4.(b) give the changes of polarization components in x_3 direction and in x_2 direction, respectively, at x_2 = 0 in Fig.3. The polarization component P_3 near the crack with zero-polarization boundary condition is smaller than that of free-polarization boundary condition as shown in Fig.4.(a). In the area far from the crack, the results from the two boundary conditions become the same. The polarization component P_2 with zero-polarization is positive below the crack, while it becomes negative above the crack as shown in Fig.4.(b). The curve with zero-polarization is anti-symmetrical with respect to the line x_3 = 0. The trend of the change is different from that of free-polarization.

Fig.5.(a) and Fig.5.(b) show the polarization distributions around electrically semi-permeable cracks filled with water for the free-polarization and zero-polarization boundary conditions, respectively. It can be found that the results are similar to those of the permeable crack in Fig.3. These results imply that when a ferroelectric crack is filled with water or other fluid with higher dielectric constant than water, it can be regarded as an electrically permeable crack. Fig.6.(a) and Fig.6.(b) show the polarization distributions around electrically semi-permeable cracks filled with silicon oil for the free-polarization and zero-polarization boundary conditions, respectively. For the crack with silicon oil, the crack has some influences on the orientation of the polarization vectors even in the condition of free-polarization as shown in Fig.6.(a). It is interesting that the polarization vectors above and below the crack change orientation greatly and form small polarization vortices under the zero-polarization boundary condition as shown in Fig.6.(b). The influence of crack on the polarization distribution becomes significant when the dielectric constant of the fluid in the crack further increases. This can be seen from Fig.7 where the crack is filled with air. Fig.7.(a) and Fig.7.(b) show the polarization distributions around electrically semi-permeable cracks filled with air for the free-polarization and zero-polarization boundary conditions, respectively. For both free-polarization and zero-polarization boundary conditions, the crack has a significant influence on the polarization distribution. Four polarization vortices can be found from both cases. The crack filled with air approaches an impermeable crack. This can be confirmed by the results in Fig.8, which is an electrically impermeable crack.

Fig.9. gives the change of polarization components in x_3 direction at $x_2 = 0$ for the cracks with different electrical boundary conditions. Fig.9.(a) and Fig.9.(b) show the results for the free-polarization and zero-polarization boundary conditions, respectively. It can be found that the impermeable crack has the largest influence and the permeable crack has the

smallest influence on the polarization for both the free-polarization and zero-polarization boundary conditions. For zero-polarization boundary condition, the permeable crack and the crack with water have almost the same influence on the polarization as shown in Fig.9.(b). Fig.10(a) shows the change of polarization components in x_2 direction at x_2 = 17 in front of cracks with different electrical boundary conditions for the free-polarization boundary condition. It can be found that the impermeable crack and the cracks with air and oil have the similar influence on the polarization. But the permeable crack and the crack with water have different influences on the polarization. The permeable crack has the smallest influence on the polarization. For zero-polarization boundary condition, however, the permeable crack and the crack with water have the same influence on the polarization as shown in Fig.10(b). From Fig.10(b), it can also be found that the cracks with different electrical boundary conditions have the similar influence on polarization component P_2 in front of crack.

6. Concluding remarks

To conclusion, a phase field model is employed to study the polarization distribution around an open crack with different electrical boundary conditions in a single crystal ferroelectric with single domain. The phase field model is based on a three-dimensional nonlinear finite element method for ferroelectric materials, which includes three physical fields, namely polarization field, electric field and strain field. The new feature of the present model is to taken into account the surface effect on the polarization on crack surfaces, which has not been studied before. It is found that the impermeable crack and the crack filled with air have a significant influence on the polarization distribution while the permeable and the crack filled with water have little influence on the polarization distribution in the ferroelectrics. It is also found that the zero boundary condition of polarization increases the

influence of the crack on the polarization distribution for the permeable crack and the crack filled with water. The results in the present study suggest that a crack filled with air can be approximated as an impermeable crack and a crack filled with water can be regarded as a permeable crack in ferroelectric materials.

Acknowledgements

JW gratefully acknowledges the support from the Alexander von Humboldt Foundation, Chinese Universities Scientific Fund, and Nature Science Foundation of China No. 10832009.

References

[1] Wang J, Kamlah M. Three-dimensional finite element modeling of polarization switching in a ferroelectric single domain with an impermeable notch. Smart Mater Struct 2009;18:104008 (1-8).

[2] Suo Z, Kuo CM, Barnett DM, Willis JR. Fracture mechanics for piezoelectric ceramics. J Mech Phys Solid 1992;40:739–65.

[3] Zhang TY, Zhao MH, Tong P. Fracture of piezoelectric ceramics. Adv Appl Mech 2002;38:147–289.

[4] Hao T-H, Shen Z-Y. A new electric boundary condition of electric fracture mechanics and its application. Engng Fract Mech 1994;47:793–802.

[5] Landis CM. Energetically consistent boundary conditions for electromechanical fracture. Int J Solid Struct 2004;41:6291–315.

[6] Gruebner O, Kamlah M, Munz D. Finite element analysis of cracks in piezoelectric materials taking into account the permittivity of the crack medium. Engng Fract Mech 2003;70:1399–413.

[7] Ricoeur A, Enderlein M, Kuna M. Calculation of the J-integral for limited permeable

cracks in piezoelectrics. Arch Appl Mech 2005;74:536–49.

[8] Park S, Sun C. Facture criteria for piezoelectric ceramics. J Am Ceram Soc 1995;78:1475-1480.

[9] Fu R, Zhang T. Effects of an electric field on the fracture toughness of poled lead zirconate titanate ceramics. J Am Ceram Soc. 2000;83:1215-1218.

[10] Hwang S, Lynch C, McMeeking R. Ferroelectric/ferroelastic interactions and a polarization switching model. Acta Metal Mater. 1995:43:2073-2084.

[11] Huber J, Fleck N, Landis C, McMeeking R. A constitutive model for ferroelectric polycrystals. J Mech Phys Solids. 1999:47:1663-1697.

[12] Kamlah M, Tsakmakis C. Phenomenological modeling of the non-linear electromechanical coupling in ferroelectrics. Int J Solids Struct 1999;36:669-695.

[13] Mehling V, Tsakmakis C, Gross D. Phenomenological model for the macroscopical material behavior of ferroelectric ceramics. J. Mech. Phys. Solids, 2007;55:2106-2141.

[14] Wang J, Shi S, Chen L, Li Y, Zhang T. Phase field simulations of ferroelectric/ferroelastic polarization switching. Acta Mater. 2004;52:749-764.

[15] Schrade D, Mueller R, Xu B, Gross D. Domain evolution in ferroelectric materials: A continuum phase field model and finite element implementation. Comput Methods Appl Mech Eng 2007;196:4365-4374.

[16] Su Y, Landis C. Continuum thermodynamics of ferroelectric domain evolution: Theory, finite element implementation, and application to domain wall pinning. J Mech Phys Solids. 2007 ;55:280-305.

[17] Wang J, Kamlah M. Intrinsic switching of polarization vortex in ferroelectric nanotubes. Physical Review B 2009;80:012101(1-4)

[18] Wang J, Kamlah M. Domain control in ferroelectric nanodots through surface charges. Applied Physics Letters. 2008;93:262904 (1-3).

[19] Vendik OG, Zubko SP. Ferroelectric phase transition and maximum dielectric

permittivity of displacement type ferroelectrics (Ba(x)Sr(1-x)TiO3). J Appl Phys 2000;88:5343-5350.

[20] Cao W, Cross L. Theory of tetragonal twin structures in ferroelectric perovskites with a first-order phase transition. Phys Rev B 1991;44:5-12.

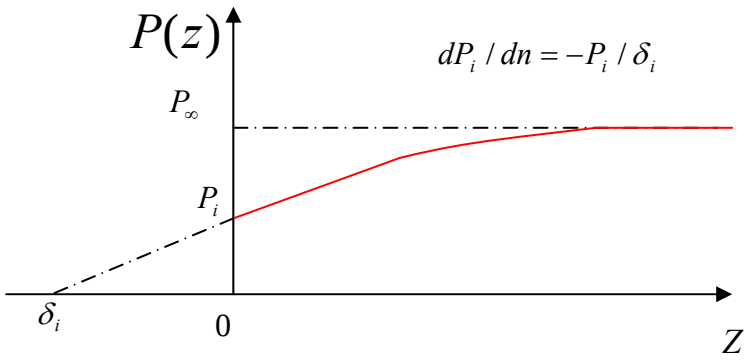

Fig.1. The surface effect of polarization on ferroelectric surface, in which P_i and P_∞ are the polarization at the surface and the inside of the ferroelectrics, respectively.

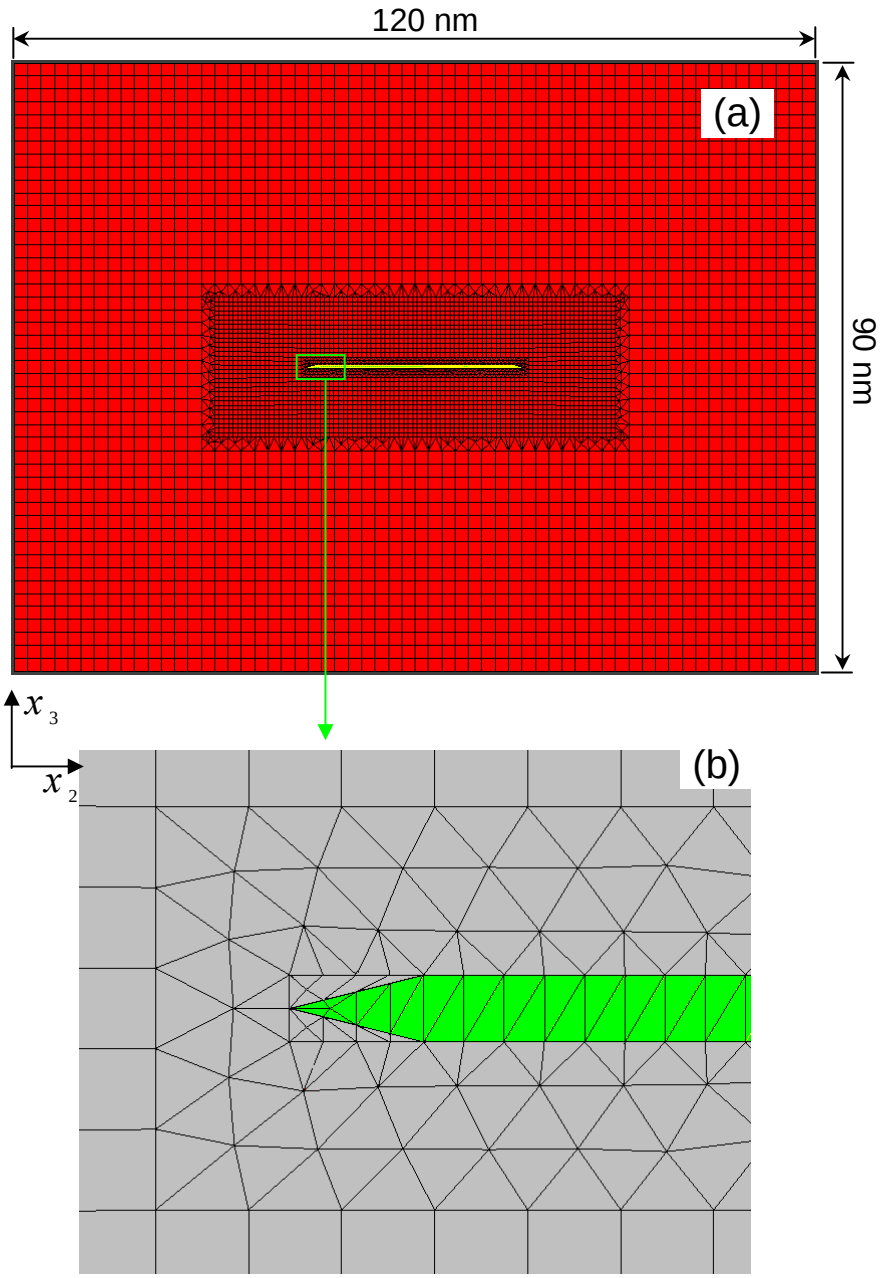

Fig.2. Mesh partition of the simulated ferroelectric single crystal plate with a crack in the middle. (a) Global mesh; (b) Refined mesh around the crack tip (the green area denotes the crack). The crack is also partitioned and is assumed to be filled with fluids. The initial polarization of P_o=0.757 C/m^2 is along x_3 positive direction. The upper and lower boundaries of the ferroelectric plate are short-circuited and other boundaries are open-circuited so that the initial polarization is uniform and stable if there is no crack. All boundaries of the ferroelectric plate are assumed to be stress-free.

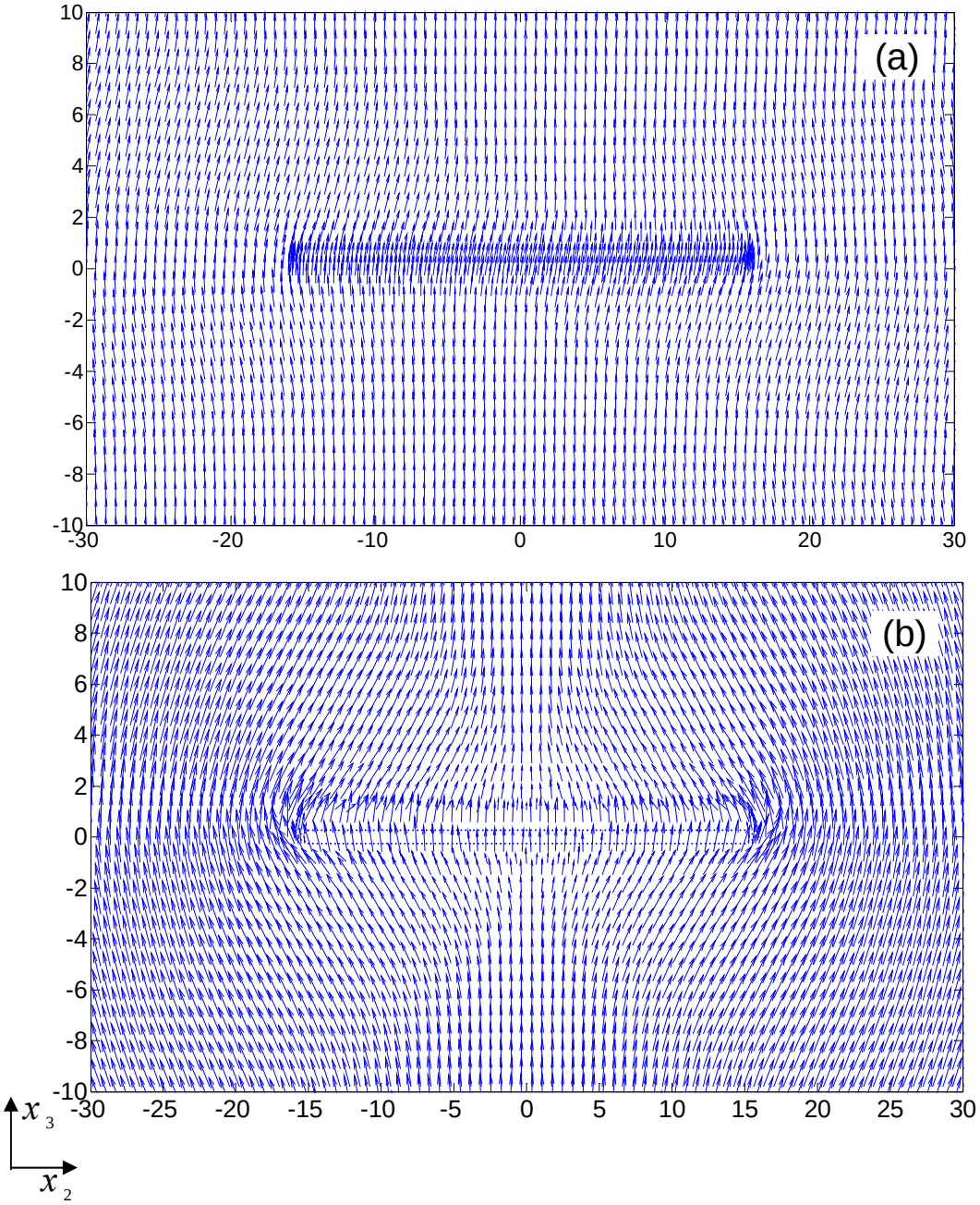

Fig.3. Polarization distributions around electrically permeable cracks with (a) free-polarization and (b) zero-polarization boundary conditions. All units are nanometer in the figure.

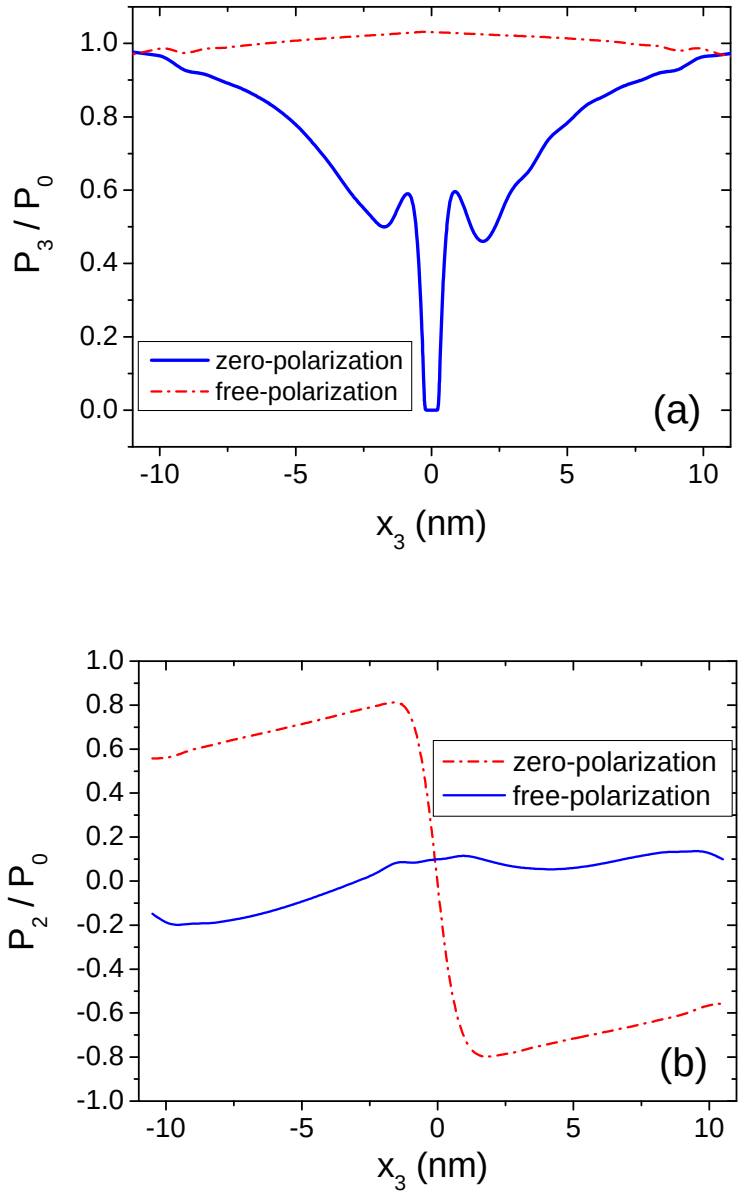

Fig.4. Change of polarization components (a) in x_3 direction and (b) in x_2 direction at $x_2 = 0$ (in the middle of crack) in Fig.3.

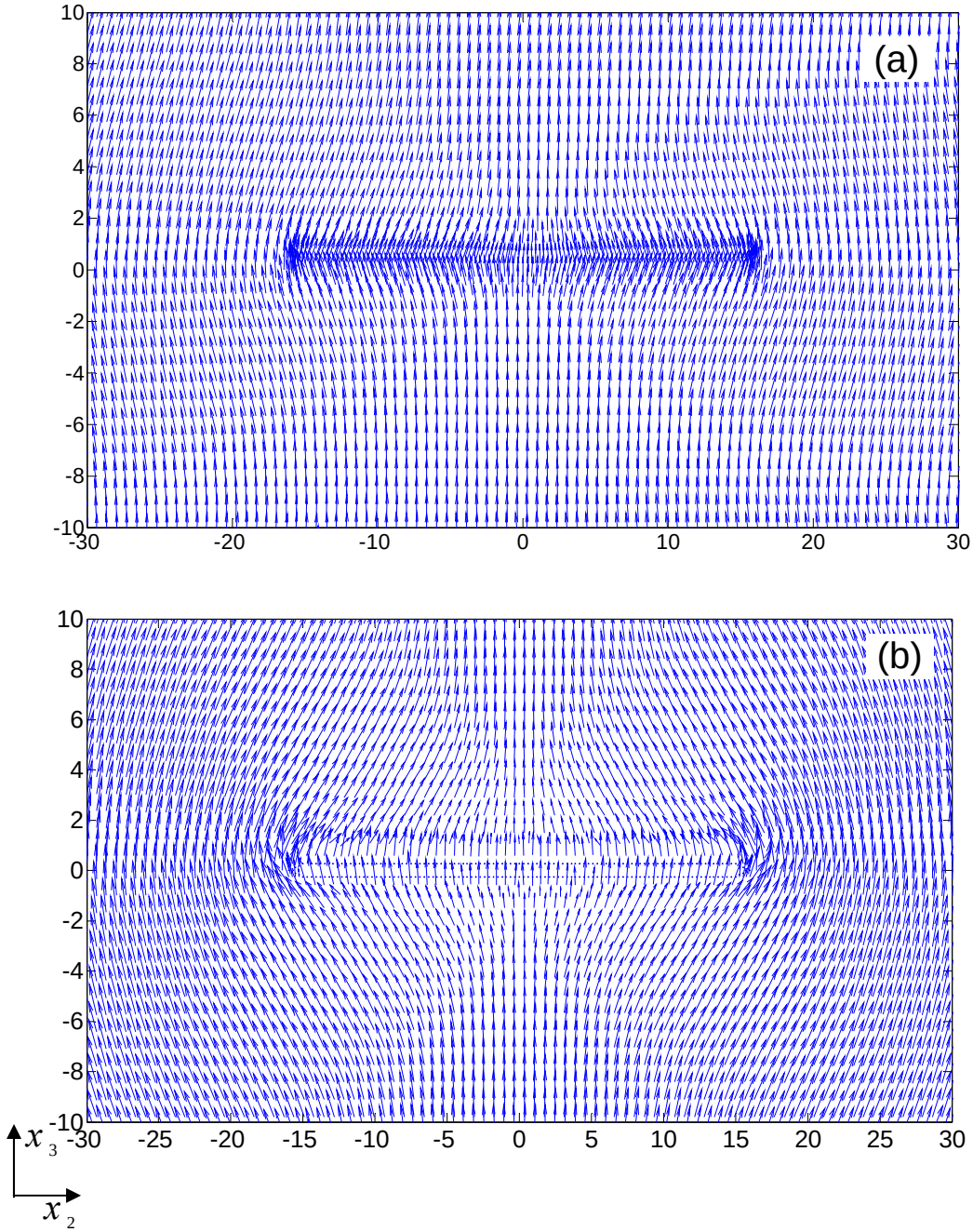

Fig.5. Polarization distributions around cracks filled with water and with (a) free-polarization and (b) zero-polarization boundary conditions.

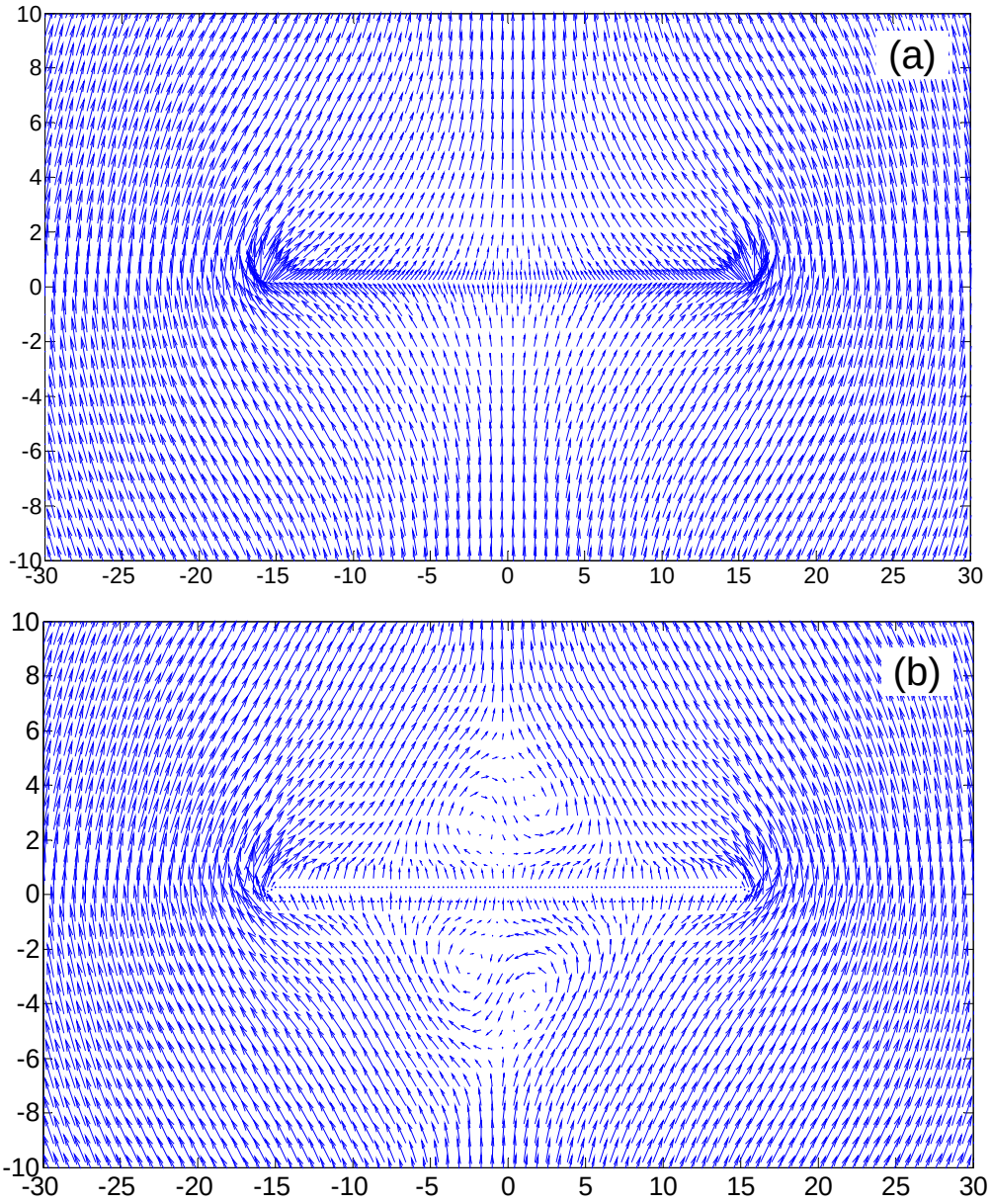

Fig.6. Polarization distributions around cracks filled with silicon oil and with (a) free-polarization and (b) zero-polarization boundary conditions.

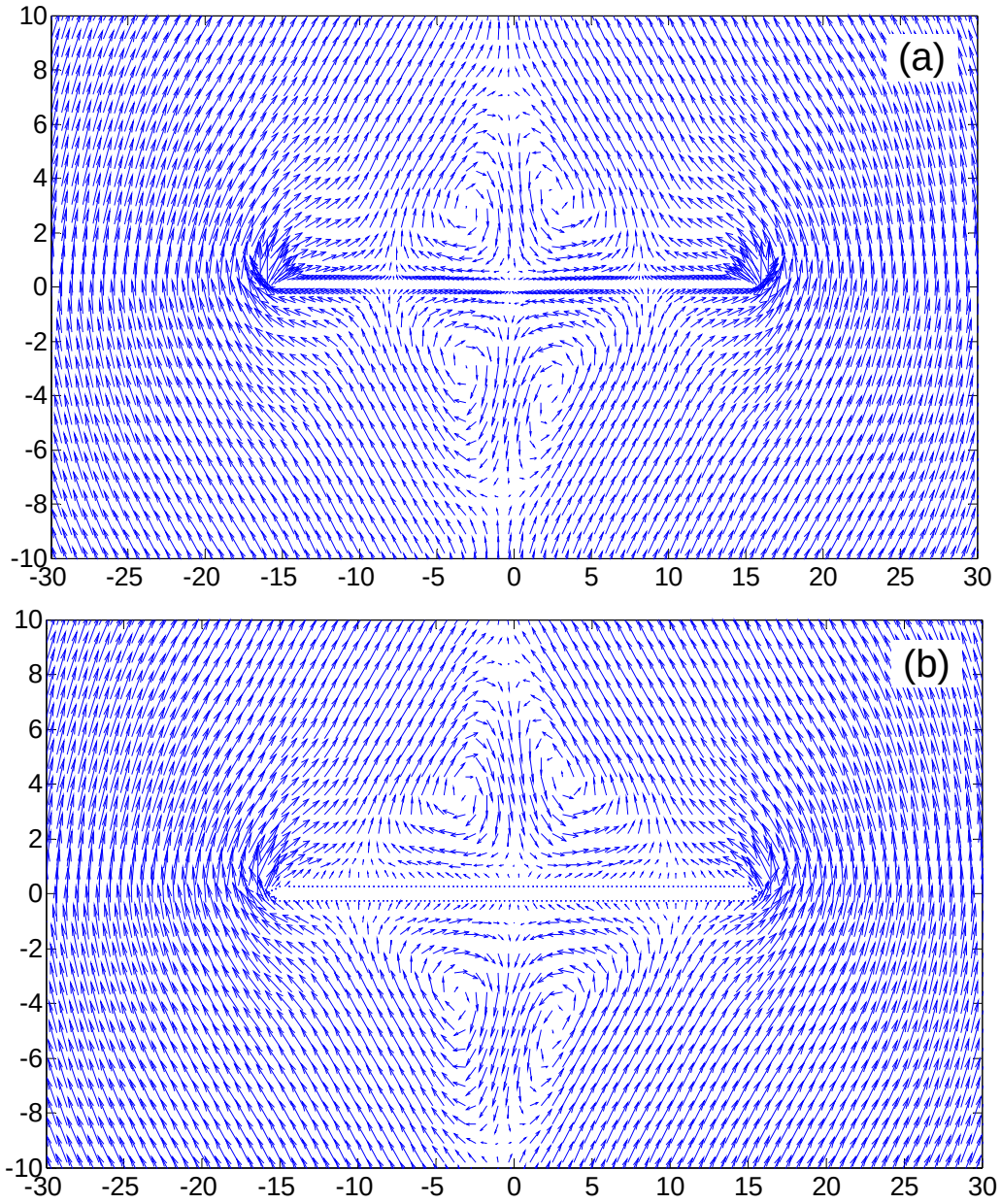

Fig.7. Polarization distributions around cracks filled with air and with (a) free-polarization and (b) zero-polarization boundary conditions.

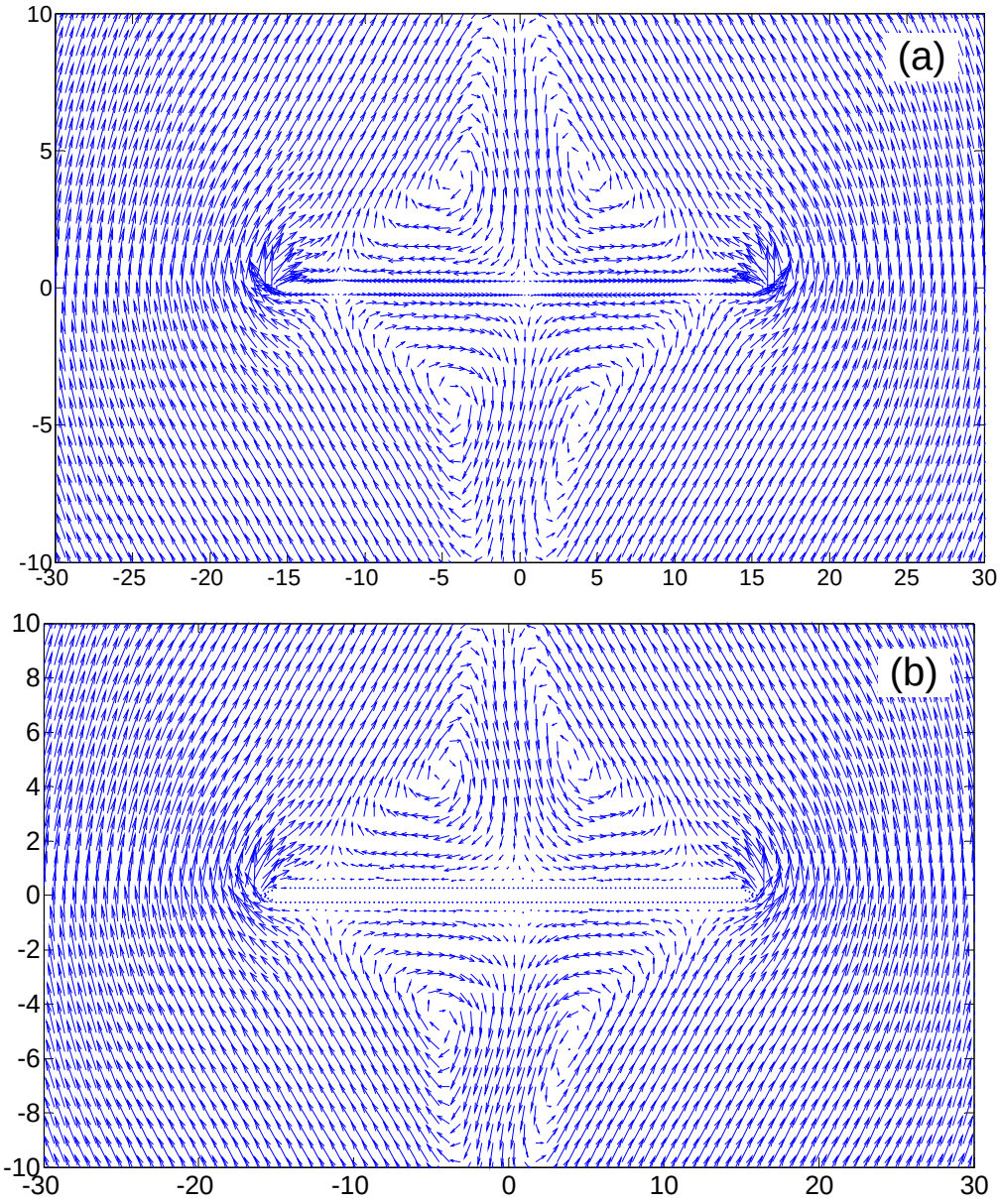

Fig.8. Polarization distributions around electrically impermeable cracks with (a) free-polarization and (b) zero-polarization boundary conditions.

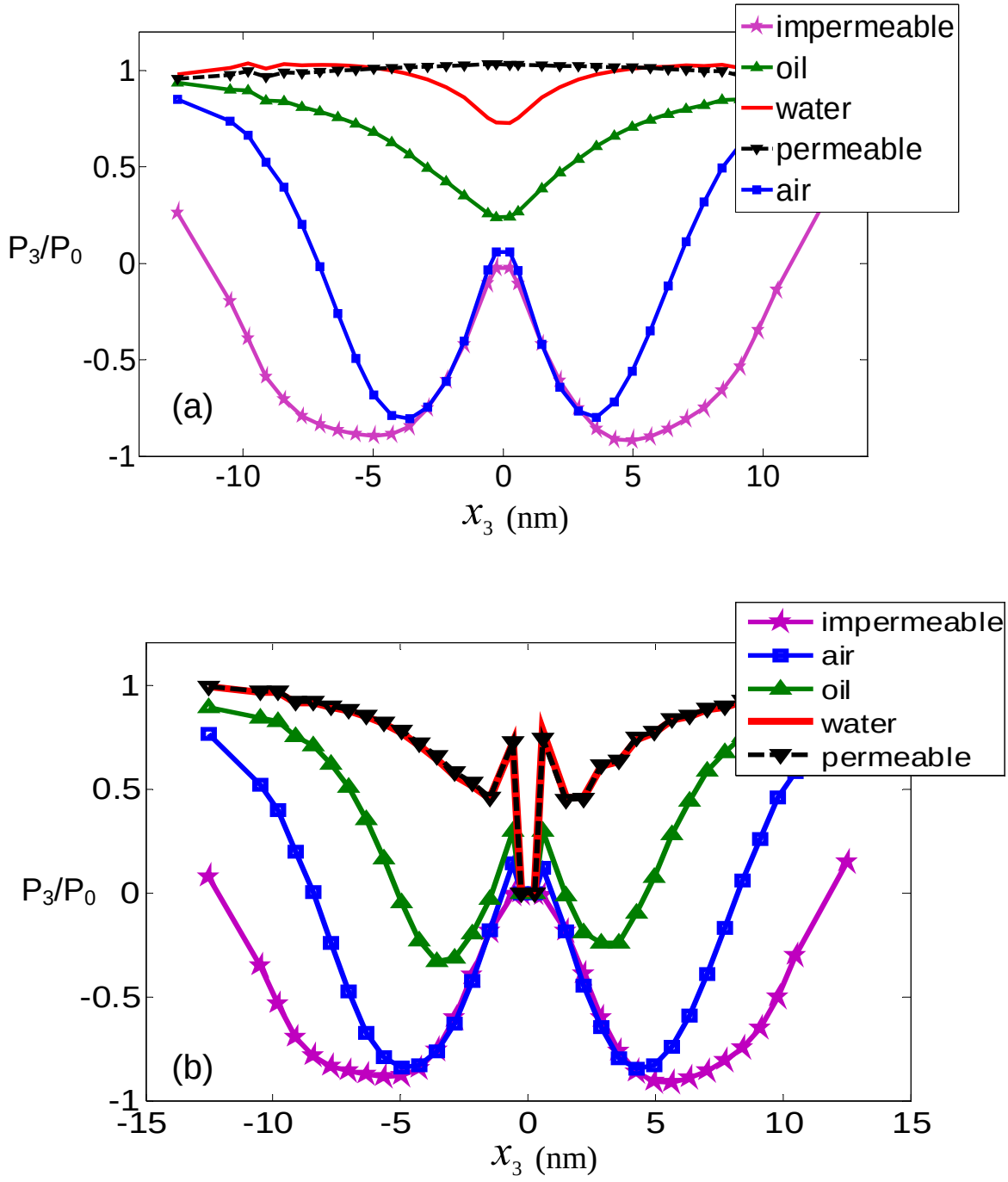

Fig.9. Change of polarization components in x_3 direction at $x_2 = 0$ (in the middle of crack) in Fig.3, Fig.5, Fig.6, Fig.7 and Fig.8 for different cracks. (a) free-polarization; (b) zero-polarization.

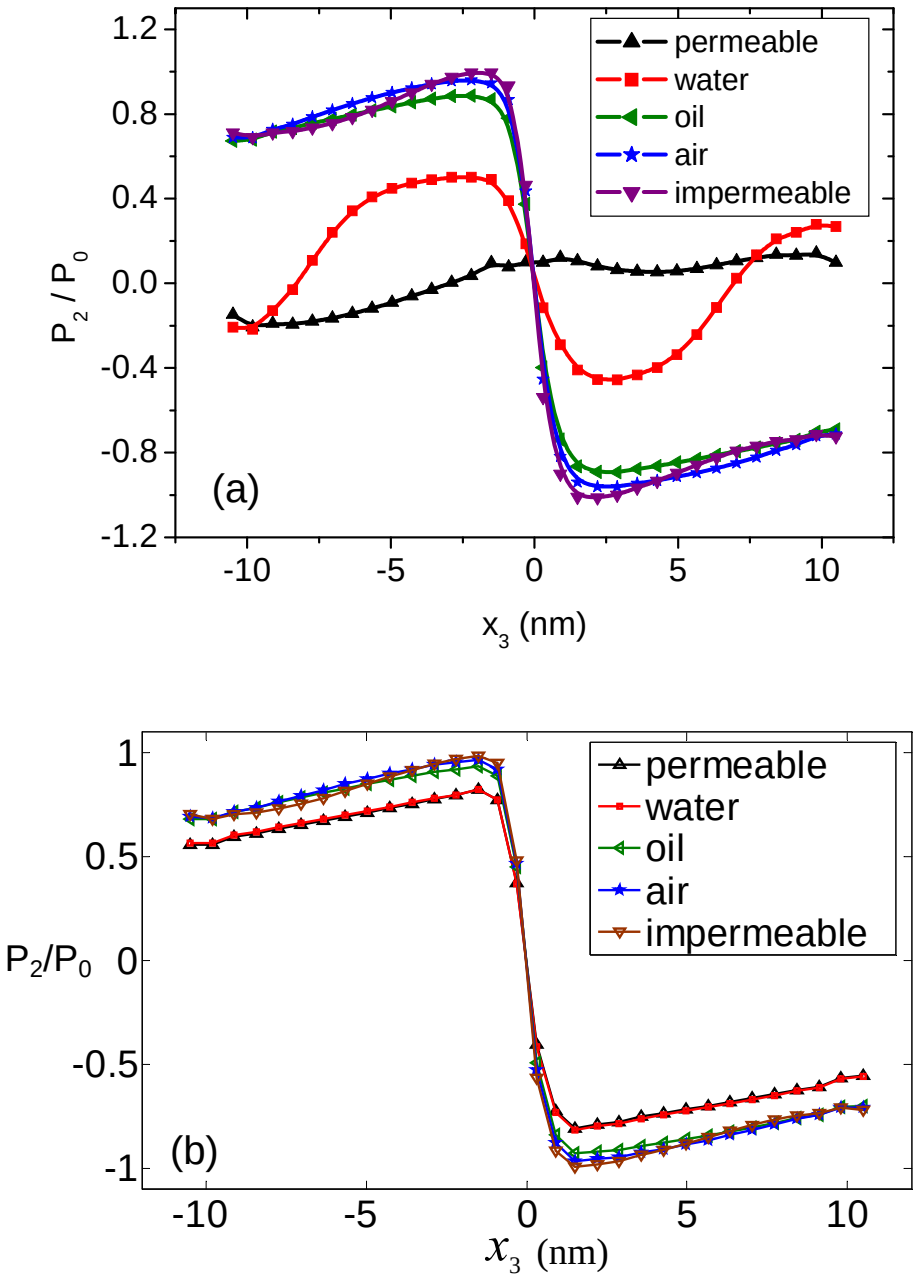

Fig.10. Change of polarization components in x_2 direction at x_2 = 17 nm (in front of crack) in Fig.3, Fig.5, Fig.6, Fig.7 and Fig.8 for different cracks. (a) free-polarization; (b) zero-polarization.